

Scalar dark matter and Muon $g - 2$ in a $U(1)_{L_\mu - L_\tau}$ model

XINXIN QI,¹ AIGENG YANG,¹ WEI LIU,² and HAO SUN^{1,*}

¹*Institute of Theoretical Physics, School of Physics, Dalian University of Technology,
No.2 Linggong Road, Dalian, Liaoning, 116024, People's Republic of China*

²*Department of Applied Physics, Nanjing University of Science and Technology,
Nanjing 210094, People's Republic of China*

We consider a simple scalar dark matter model within the frame of gauged $L_\mu - L_\tau$ symmetry. A gauge boson Z' as well as two scalar fields S and Φ are introduced to the Standard Model (SM). S and Φ are SM singlet but both with $U(1)_{L_\mu - L_\tau}$ charge. The real component and imaginary component of S can acquire different masses after spontaneously symmetry breaking, and the lighter one can play the role of dark matter which is stabilized by the residual Z_2 symmetry. A viable parameter space is considered to discuss the possibility of light dark matter as well as co-annihilation case, and we present current $(g - 2)_\mu$ anomaly, Higgs invisible decay, dark matter relic density as well as direct detection constraints on the parameter space.

I. INTRODUCTION

Recently, the Fermi-lab reported a new measurement from the Muon $g - 2$ experiment [1–3], the result is:

$$a_\mu^{\text{exp}} = 116592061(41) \times 10^{-11}, \quad (1)$$

compared with the SM prediction

$$a_\mu^{\text{SM}} = 116591810(43) \times 10^{-11}. \quad (2)$$

The observed 4.2σ discrepancy raises a big challenge to the SM and can give us new hints to the new physics. Models related with $(g - 2)_\mu$ anomaly can be found in [4–14]. Among these models, the gauged $U(1)_{L_\mu - L_\tau}$ has been discussed for a long time for its simplicity since anomaly cancellation can be accomplished without introducing new fermions in such model. Discussion about models for a new gauge boson (Z') can be found in [15–22], where the $(g - 2)_\mu$ anomaly can be naturally explained by the one loop contribution of Z' , and the new gauge boson mass is limited to be not too heavy. Searches for Z' at experiment can give the most stringent limit on the gauge boson mass and coupling constant, and a viable parameter space with Z' boson mass at MeV scale has been well studied, which also satisfies current experiment constraints [23–26].

The gauged $U(1)_{L_\mu - L_\tau}$ symmetry gives possible direction for the extension of SM, and one can introduce new extra particles with $U(1)_{L_\mu - L_\tau}$ charge to the model to explain dark matter problem, which is also a huge challenge to the SM. According to the astronomical observation, our universe is not just composed of SM particles, but also dark matter as well as dark energy [27]. Dark matter particles are assumed to be electrically neutral, colorless and stable on cosmological scales. To explain the observed relic density of dark matter, thermal Freeze-out [28] and Freeze-in [29] mechanism have been

put forward. Aside from dark matter annihilating into SM particles, other processes such as semi-annihilation [30] and co-annihilation [31], can also contribute to the relic density of dark matter. New fermions as dark matter candidate in a gauged $L_\mu - L_\tau$ model can be found in [32, 33], while scalar dark matter models have been discussed in [34, 35], where the current relic density is obtained via Freeze-in mechanism. Among these models, dark matter particles are almost stabilized by $U(1)_{L_\mu - L_\tau}$ symmetry. Besides these models, one can also consider a type of so-called darkon DM matter model [36, 37]. The darkon can play the role of dark matter via its lighter component after spontaneously symmetry breaking in the case of $U(1)$ extension of the SM [38–40]. Particularly, one can have co-annihilation contribution when the real component and imaginary component of darkon are nearly degenerate.

In this article, we consider a simple scalar dark matter model within the frame of the gauged $L_\mu - L_\tau$ symmetry. We introduce a new gauge boson Z' and two scalar fields S and Φ to the SM, S and Φ are singlet in the SM but carry $U(1)_{L_\mu - L_\tau}$ charge. The scalar Φ will spontaneously breaking so that the new gauge boson Z' acquires mass, while the lighter component of S will play the role of dark matter in our model after spontaneously breaking, which will be stabilized with the residual Z_2 symmetry. We focus on the $(g - 2)_\mu$ anomaly problem and scalar dark matter in this work, and discussion about neutrino mass problem in a similar gauged $L_\mu - L_\tau$ model can be found in [41], where the scalar dark matter in this model is stabilized by $U(1)_{L_\mu - L_\tau}$ symmetry. We consider the possibility of light dark matter as well as co-annihilation case in our model and we show the Higgs invisible decay, relic density constraint as well as direct detection constraint on a viable parameter space.

This article is arranged as followed: We give the description of the scalar dark matter model in section II. We consider the $(g - 2)_\mu$ anomaly constraint on the parameter space in section III. We discuss Higgs invisible decay, relic density as well as direct detection constraint on the chosen parameter space separately in IV A, IV B and IV C. We give a summary in the last section V.

*Electronic address: haosun@dlut.edu.cn

II. MODEL DESCRIPTION

We discuss a scalar dark matter model based on the $U(1)_{L_\mu-L_\tau}$ extension of the SM. A new gauge boson Z' as well as two SM singlet scalar Φ and S are introduced to the standard model. The field H gives the non-zero vacuum expectation value (vev) like in the SM, while Φ develops a vev to break the $U(1)_{L_\mu-L_\tau}$ symmetry. The field S has zero vev and plays the role of scalar dark matter via its lighter component. Z' will acquire mass after symmetry breaking spontaneously. We can assume S and Φ carry opposite $U(1)_{L_\mu-L_\tau}$ charge so that we have $\lambda_{ds}(S^2\Phi^2 + S^{\dagger 2}\Phi^{\dagger 2})$ in the lagrangian, which is essential because it triggers the $U(1)_{L_\mu-L_\tau} \rightarrow Z_2$ spontaneously breakdown as soon as Φ acquires a vev.

The additional part of the fermion lagrangian is given by:

$$\mathcal{L}_{\text{fermion}} = g_p Z'^\sigma (\bar{\mu}\gamma^\sigma \mu - \bar{\tau}\gamma^\sigma \tau + \bar{\nu}_\mu\gamma^\sigma P_L \nu_\mu - \bar{\nu}_\tau\gamma^\sigma P_L \nu_\tau). \quad (3)$$

The scalar part with dark matter is given by:

$$\mathcal{L}_{\text{scalar}} = |D_\mu \Phi|^2 + |D_\mu H|^2 + |D_\mu S|^2 - \mathcal{V}(H, \Phi, S) \quad (4)$$

with

$$\begin{aligned} D_\mu \Phi &= \partial_\mu \Phi - ig_p q_1 A'_\mu \Phi, \\ D_\mu H &= \partial_\mu H - ig_L W_\mu H - \frac{i}{2} g_Y A_\mu H, \\ D_\mu S &= \partial_\mu S - ig_p q_2 A'_\mu S, \end{aligned} \quad (5)$$

where q_1 and q_2 are the $U(1)_{L_\mu-L_\tau}$ charge of Φ and S , g_p is the $U(1)_{L_\mu-L_\tau}$ coupling constant. For simplicity, we assume $q_1 = 2$ and $q_2 = -2$ as we considered above. The potential term $\mathcal{V}(H, \Phi, S)$ is given by:

$$\begin{aligned} \mathcal{V}(H, \Phi, S) &= \mu |H|^2 + \lambda_H |H|^4 + \mu_1 |\Phi|^2 + \lambda_p |\Phi|^4 \\ &\quad - \frac{1}{2} m_0^2 |S|^2 + \frac{\lambda_s}{4} |S|^4 + \lambda_{Hp} |H|^2 |\Phi|^2 \\ &\quad + \lambda_{Hs} |H|^2 |S|^2 + \lambda_{SP} |S|^2 |\Phi|^2 \\ &\quad + \frac{\lambda_{ds}}{2} (S^2 \Phi^2 + S^{\dagger 2} \Phi^{\dagger 2}). \end{aligned} \quad (6)$$

where $\mu < 0$ and $\mu_1 < 0$ and $m_0^2 > 0$. We assume H and Φ spontaneously breaking, and we have H and Φ in unitary gauge form with:

$$H = \begin{pmatrix} 0 \\ \frac{v+h}{\sqrt{2}} \end{pmatrix}, \quad \Phi = \frac{v_b + \phi}{\sqrt{2}} \quad (7)$$

where v and v_b are the vevs and we assume v is the SM one equal 246 GeV. What's more, $v_b = M_{Z_p}/2g_p$, where M_{Z_p} is the new gauge boson Z' mass. Furthermore, we can write $S = S_R + iS_I$ in the form of real component and imaginary component, and we have:

$$m_R^2 = m_0^2 + \lambda_{SP} v_b^2 + \lambda_{Hs} v^2 + \lambda_{ds} v_b^2 \quad (8)$$

$$m_I^2 = m_0^2 + \lambda_{SP} v_b^2 + \lambda_{Hs} v^2 - \lambda_{ds} v_b^2 \quad (9)$$

where m_R^2, m_I^2 correspond to the squared mass of S_R and S_I . The mass difference between S_R and S_I is determined by the sign of λ_{ds} . We can take $\lambda_{ds} > 0$ so that the lighter particle S_I is the weakly interacting massive particle (WIMP) dark matter. The result will be the same if we take $\lambda_{ds} < 0$ while S_R acts as the dark matter.

The mass matrix related with two Higgs is given by the following, after spontaneously breaking:

$$\mathcal{M} = \begin{pmatrix} 2\lambda_H v^2 & \lambda_{Hp} v v_b \\ \lambda_{Hp} v v_b & 2\lambda_p v_b^2 \end{pmatrix}. \quad (10)$$

The mass matrix eigenvalue can be analytically expressed, and the result is given by:

$$m_1^2 = \lambda_H v^2 + \lambda_p v_b^2 - \sqrt{(\lambda_H v^2 - \lambda_p v_b^2)^2 + \lambda_{Hp}^2 v_b^2 v^2} \quad (11)$$

$$m_2^2 = \lambda_H v^2 + \lambda_p v_b^2 + \sqrt{(\lambda_H v^2 - \lambda_p v_b^2)^2 + \lambda_{Hp}^2 v_b^2 v^2}. \quad (12)$$

The gauge eigenstate and mass eigenstate is related with a mixing angle θ which can be determined

$$\sin 2\theta = \frac{\lambda_{Hp} v v_b}{\sqrt{(\lambda_H v^2 - \lambda_p v_b^2)^2 + \lambda_{Hp}^2 v_b^2 v^2}}. \quad (13)$$

We consider the lighter Higgs is just the SM Higgs observed at the LHC with $m_1 = 125\text{GeV}$ and m_2 being another Higgs mass in this work. We use h_1 to represent the SM Higgs and h_2 to represent another Higgs for convenience. The relation between the mass eigenstates and mass eigenstates can be given by:

$$\begin{pmatrix} h_1 \\ h_2 \end{pmatrix} = \begin{pmatrix} \cos \theta & -\sin \theta \\ \sin \theta & \cos \theta \end{pmatrix} \begin{pmatrix} h \\ \phi \end{pmatrix} \quad (14)$$

and we can express the couplings with two Higgs mass and mixing angle as followed:

$$\lambda_H = \frac{m_1^2}{4v^2}(1 + \cos 2\theta) + \frac{m_2^2}{4v_b^2}(1 - \cos 2\theta) \quad (15)$$

$$\lambda_p = \frac{m_1^2}{4v_b^2}(1 - \cos 2\theta) + \frac{m_2^2}{4v^2}(1 + \cos 2\theta) \quad (16)$$

$$\lambda_{Hp} = \sin 2\theta \frac{m_2^2 - m_1^2}{2v v_b}. \quad (17)$$

To make sure the model perturbative, contribution from loop correction should be smaller than tree level values, such constraint can be ensured when [42]

$$\begin{aligned} |\lambda_H| &< 4\pi, \quad |\lambda_{Hp}| < 4\pi, \quad |\lambda_p| < 4\pi, \quad |\lambda_{Hs}| < 4\pi, \\ |\lambda_{ds}| &< 4\pi, \quad |\lambda_{SP}| < 4\pi. \end{aligned} \quad (18)$$

What's more, to obtain a stable vacuum, the quartic couplings appearing in the lagrangian should be

constrained, we consider the necessary and sufficient conditions as followed [43, 44]:

$$\begin{aligned}
&\lambda_H \geq 0, \lambda_s \geq 0, \lambda_p \geq 0, \lambda_{Hs} \geq -2\sqrt{\lambda_H \lambda_s}, \\
&\lambda_{Hp} \geq -2\sqrt{\lambda_H \lambda_p}, \lambda_{SP} \geq -2\sqrt{\lambda_p \lambda_s}, \\
&\sqrt{\lambda_{Hs} + 2\sqrt{\lambda_H \lambda_s}} \sqrt{\lambda_{Hp} + 2\sqrt{\lambda_H \lambda_p}} \sqrt{\lambda_{SP} + 2\sqrt{\lambda_p \lambda_s}} \\
&+ 2\sqrt{\lambda_H \lambda_s \lambda_p} + \lambda_{Hp} \sqrt{\lambda_s} + \lambda_{Hs} \sqrt{\lambda_p} \\
&+ \lambda_{SP} \sqrt{\lambda_H} \geq 0.
\end{aligned} \tag{19}$$

In this work, we choose the following parameters as the inputs with

$$m_2, M_{Z_p}, g_p, \lambda_s, \lambda_{ds}, \lambda_{SP}, \lambda_{Hs}, \sin \theta, m_0. \tag{20}$$

III. PARAMETER CONSTRAINTS ON Z'

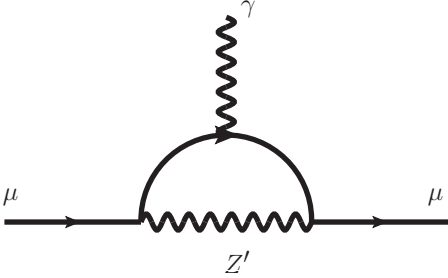


FIG. 1: One-loop contribution of Z' to $(g-2)_\mu$ anomaly.

Before discussion, we should consider the $(g-2)_\mu$ constraints on $M_{Z_p} - g_p$ plane, since one prospect to introduce $U(1)_{L_\mu - L_\tau}$ symmetry is to explain the $(g-2)_\mu$ anomaly. Contribution of the new gauge boson Z' to the muon anomalous magnetic momentum is shown in Figure 1. The analytical expression for Δa_μ is

$$\Delta a_\mu = \frac{g_p^2 m_\mu^2}{8\pi^2} \int_0^1 \frac{2x^2(1-x)}{x^2 m_\mu^2 + (1-x)M_{Z_p}^2} dx \tag{21}$$

where m_μ is the muon mass.

Searches for new gauge bosons at experiment has already given the most stringent constraint on the parameter space of $M_{Z_p} - g_p$. At colliders, the Z' gauge boson can be produced via $e^+e^- \rightarrow \mu^+\mu^-Z'$ with the subsequent decay of $Z' \rightarrow \mu\mu$. Such search can be found in Babar [23] and give us the possible bound on $M_{Z_p} - g_p$ plane. What's more, neutrino experiments give us new clues to constrain the parameter space. The Borexino data related with the scattering of low energy solar neutrinos [45, 46] can provide the most stringent constraint on the low M_{Z_p} and low g_p region. Another constraint is from CCFR collaboration [47], obtained via the neutrino trident production which is related with the process $\nu N \rightarrow \nu N \mu^+ \mu^-$, where a muon neutrino

scattered off of a nucleus producing a $\mu^+ \mu^-$ pair. Such process will be enhanced due to the existence of Z' compared with SM case, which gives strong bounds on the possible Z' contribution and constrain the $M_{Z_p} - g_p$ parameter space accordingly. In our paper, we focus on

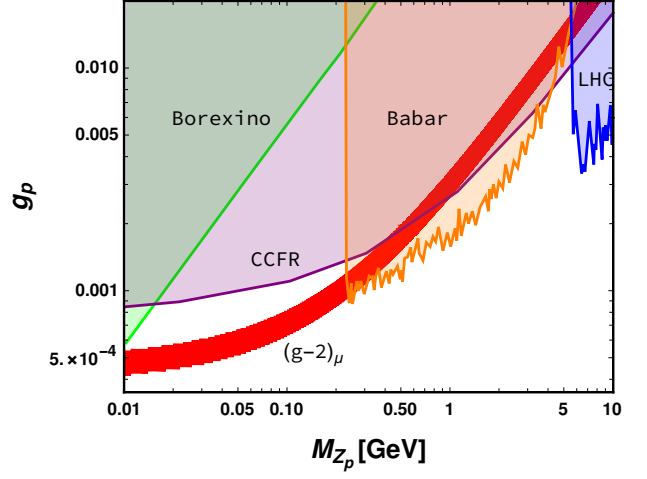


FIG. 2: The allowed region that can explain the $(g-2)_\mu$ anomaly and the excluded region on $M_{Z_p} - g_p$ from different experiments: the green (orange, blue, purple) region is excluded by the Borexino (BABAR, LHC, CCFR). The red region is the parameter satisfying $(g-2)_\mu$ anomaly.

the low M_{Z_p} region. The combined experiment as well as $(g-2)_\mu$ constraints on the $M_{Z_p} - g_p$ is given in Figure 2. According to Figure 2, CCFR gives the most stringent constraint on the parameter space we interest at low M_{Z_p} region. The Borexino limits become relevant at smaller M_{Z_p} and g_p . For $M_{Z_p} \in [0.2, 5]$ GeV, BABAR data plays an important role to constrain M_{Z_p} and g_p .

To sum up, most of the parameter space to explain $(g-2)_\mu$ has been excluded by these experiments but $M_{Z_p} \in [0.01, 0.25]$ GeV and g_p at 10^{-3} level. The viable parameter region that can explain the $(g-2)_\mu$ anomaly in the $M_{Z_p} - g_p$ plane is shown in Figure 3 according to the latest experiment value $\Delta a_\mu = 251(59) \times 10^{-11}$ of where the red plane is the result of $\text{Log} \Delta a_\mu$ and the two yellow planes are the low bound and top bound on $\text{Log} \Delta a_\mu$ from the experiment. Intersection region of the three planes is the viable parameter space of $M_{Z_p} - g_p$ explaining $(g-2)_\mu$ anomaly, and we can give some pairs of (M_{Z_p}, g_p) with $(0.01 \text{ GeV}, 4.18 \times 10^{-4})$, $(0.25 \text{ GeV}, 1.117 \times 10^{-3})$.

IV. PHENOMENOLOGICAL STUDY

A. Higgs invisible decay

In our model, we have a new gauge boson Z' and two scalar fields S_I and S_R . We assume all these particles masses are smaller than the SM Higgs mass with $M_{Z_p} < 1/2m_1$, $m_I < 1/2m_1$ and $m_R < 1/2m_1$ so that SM

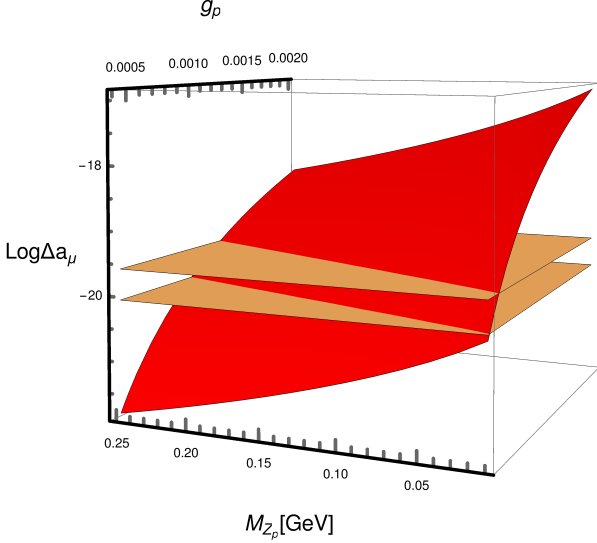


FIG. 3: $M_{Z_p} - g_p$ plane to explain $(g-2)_\mu$ anomaly with $M_{Z_p} \subseteq [0.01, 0.25]$ GeV. The red region is Log result of Eq.(21) and the two yellow regions are the latest experiment result of $(g-2)_\mu$. The overlap part of the three regions is the viable parameter space to explain $(g-2)_\mu$ anomaly within experiment constraints.

Higgs can decay to these particles which will contribute to the invisible Higgs decay width. Current constraint on such invisible branching fraction is $\text{Br}(h \rightarrow \text{inv}) < 0.24$ according to the observations at the LHC for the SM Higgs [48], which means

$$\frac{\Gamma(h \rightarrow \text{inv})}{\Gamma(h \rightarrow \text{inv}) + \Gamma(h \rightarrow \text{SM})} < 0.24. \quad (22)$$

The decay widths related with Higgs invisible decay channel in our model are given as followed:

$$\begin{aligned} \Gamma_{h_1 \rightarrow S_I S_I} &= \sqrt{m_1^2(m_1^2 - 4m_I^2)}/(8\pi m_1^3) \\ &\times (\cos \theta \lambda_{Hs} v + \lambda_{ds} \sin \theta v_b - \lambda_{SP} \sin \theta v_b)^2 \\ \Gamma_{h_1 \rightarrow S_R S_R} &= \sqrt{m_1^2(m_1^2 - 4m_R^2)}/(8\pi m_1^3) \\ &\times (\cos \theta \lambda_{Hs} v - \lambda_{ds} \sin \theta v_b - \lambda_{SP} \sin \theta v_b)^2 \\ \Gamma_{h_1 \rightarrow Z' Z'} &= g_p^4 \sqrt{m_1^2(m_1^2 - 4M_{Z_p}^2)}/(2M_{Z_p}^4 \pi m_1^3) \\ &\times (m_1^4 - 4m_1^2 M_{Z_p}^2 + 12M_{Z_p}^4) \sin^2 \theta v_b^2. \end{aligned} \quad (23)$$

In this part, we consider the Higgs invisible decay constraint on the chosen parameter space. As we can see in the following discussion, λ_{ds} is limited stringently under relic density constraint, while λ_{Hs} and λ_{SP} are more flexible. According to Eq.(22), the contribution of λ_{Hs} to Higgs invisible decay width is positive while λ_{SP} is negative. For simplicity, we can set λ_{Hs} and λ_{SP} to be some special value and give the result of the Higgs invisible decay width of our model to estimate the chosen parameter space. In Figure 4, we fixed $\lambda_{Hs} = 0.005$ and

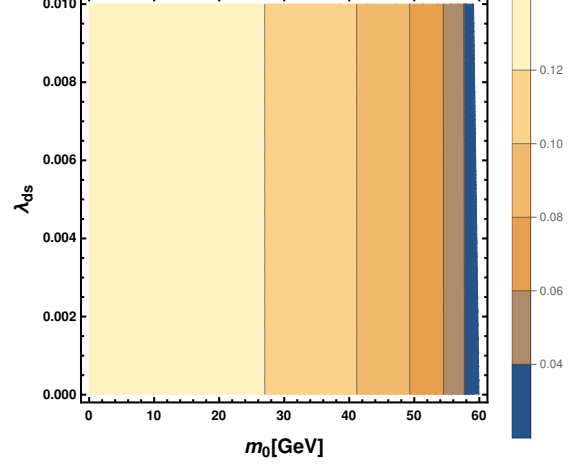


FIG. 4: Contourplot of Higgs invisible decay width where the X-axis is m_0 and Y-axis is λ_{ds} when $\lambda_{Hs} = 0.005$, $\lambda_{SP} = 0.001$.

$\lambda_{SP} = 0.001$ and set $\lambda_{ds} \subseteq [1 \times 10^{-5}, 0.01]$ and $m_0 \subseteq [0, 60] \text{ GeV}$. According to Figure 4, the Higgs invisible decay width is much lower than current constraint in the case of $\lambda_{Hs} = 0.005$ and $\lambda_{SP} = 0.001$. As we discussed above, we can set $\lambda_{Hs} < 0.005$ and $\lambda_{SP} > 0.001$ to get a viable parameter space satisfying Higgs invisible decay width constraint.

B. Relic density

In this part, we discuss the dark matter phenomenology in the model. The expression of relic abundance of dark matter can be given as followed:

$$\Omega h^2 = \frac{1.07 \times 10^9 \text{ GeV}^{-1}}{g^{*1/2} M_{Pl}} \frac{1}{J(x_f)} \quad (24)$$

where g^* is the total number of effective relativistic degrees of freedom, $M_{Pl} = 1.22 \times 10^{19}$ GeV is the Planck mass, and $J(x_f)$ is given by:

$$J(x_f) = \int_{x_f}^{\infty} \frac{dx}{x^2} \langle \sigma v \rangle (x). \quad (25)$$

The freeze-out parameter x_f in the integral is [49]:

$$x_f = \ln \frac{0.038 g M_{Pl} m_{\text{DM}} \langle \sigma v \rangle (x_f)}{(g^* x_f)^{1/2}} \quad (26)$$

where m_{DM} is the dark matter mass. According to current experiment, the dark matter relic density is [50]:

$$\Omega h^2 = 0.1198 \pm 0.0012. \quad (27)$$

Scalar dark matter in our model is stabilized by Z_2 symmetry after $U(1)_{L_\mu - L_\tau}$ symmetry spontaneously

breaking. It is worth stressed that another scalar S_R can also play role of dark matter when S_I and S_R are nearly degenerate. The dark matter relic density will not just be determined by S_I but also S_R , which is so-called co-annihilation case [51]. In the case we considered, the number density of S_R will track S_I number density during freeze-out, when the relative mass splitting Δ is small compared to the freeze-out temperature, which is defined by:

$$\Delta \equiv \frac{m_R - m_I}{m_I}. \quad (28)$$

Concretely speaking, the relic density is calculated by solving the Boltzman equation, which depends on the dimensionless variable $x = m_{\text{DM}}/T$. Freeze-out occurs at $x_F = m_{\text{DM}}/T_F \approx 20 \sim 30$ for cold, non-relativistic dark matter, where T_F is the freeze-out temperature. For $\delta m = m_R - m_I$ much larger than T_F , we have just dark matter S_I annihilations freeze-out. However, S_R will be thermally accessible when $\delta m \approx T_F$. Hence, the relative mass splitting Δ can give the upper bound that $\Delta \sim x_F^{-1} \sim 0.03 - 0.05$ when we consider the co-annihilation case. A more systematic estimate for the contribution of Δ to relic density can be found in [31]. Δ in our model can be given as followed:

$$\Delta = \frac{m_R^2 - m_I^2}{m_I(m_I + m_R)} = \frac{2\lambda_{ds}v_b^2}{m_I^2 + m_I m_R}. \quad (29)$$

According to Eq.(29), co-annihilation becomes more significant in the model as long as $\lambda_{ds} \ll m_I$, where S_I and S_R are kept in equilibrium via the interactions $S_I S_I \leftrightarrow S_R S_R$, while in the light dark matter case the main contribution of relic density arising from the annihilation of S_I . Before we consider the relic density numerically, we should stress that co-annihilation process can be dominated during the evolution of relic density in the heavy dark matter case, but we want to consider a viable region where annihilation and co-annihilation can be both involved which means the dark matter mass we considered should not be too heavy. We choose a viable parameter space with $0 \leq m_0 \leq 60$ GeV and dark matter particle mass will be constrained to be a few GeV to about 70 GeV. Annihilation process and co-annihilation will be both involved within the chosen parameter space as we can see in the following discussion.

The Feynman diagrams relevant for the dark matter production are given in Figure 5. According to Figure 5, scalar dark matter can annihilate into SM particles with Higgs-mediated interactions. In the case of $2m_{\text{DM}} > M_{Z_p}$ as we have assumed, dark matter can annihilate into a pair of Z' via t-channel as shown in Figure 5(e). Vertices related with these Feynman diagrams are given in Table I for S_I annihilation. As we have discussed above, S_R can also plays the role of dark matter in the case of co-annihilation, the relevant vertices are also given in Table I.

In this work, we use Feynrules [52] to generate implemented code, micrOmegas [53] to calculate the relic

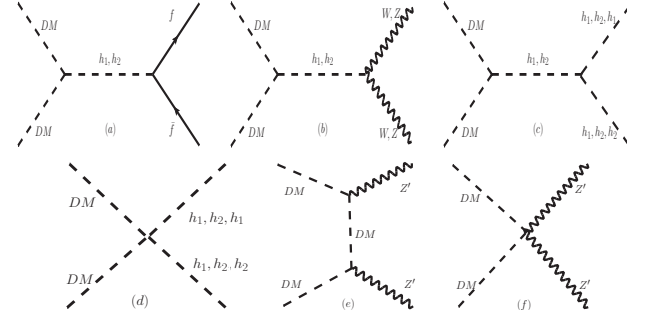


FIG. 5: Feynman diagrams related with dark matter relic density.

| Coupling | Vertex Factor |
|---|--|
| $\mathcal{C}_{S_{I(R)} S_{I(R)} h_1}$ | $-i[2v\lambda_{Hs} \cos \theta \pm 4v_b\lambda_{ds} \sin \theta \mp 2v_b\lambda_{SP} \sin \theta]$ |
| $\mathcal{C}_{S_{I(R)} S_{I(R)} h_2}$ | $-i[2v\lambda_{Hs} \sin \theta \mp 4v_b\lambda_{ds} \cos \theta \pm 2v_b\lambda_{SP} \cos \theta]$ |
| $\mathcal{C}_{S_{I(R)} S_{I(R)} h_1 h_1}$ | $-i[2\lambda_{Hs} \cos^2 \theta \mp 4\lambda_{ds} \sin^2 \theta + 2\lambda_{SP} \sin^2 \theta]$ |
| $\mathcal{C}_{S_{I(R)} S_{I(R)} h_2 h_2}$ | $-i[2\lambda_{SP} \cos^2 \theta \mp 4\lambda_{ds} \cos^2 \theta + 2\lambda_{Hs} \sin^2 \theta]$ |
| $\mathcal{C}_{S_{I(R)} S_{I(R)} h_1 h_2}$ | $-i \cos \theta \sin \theta [2\lambda_{Hs} \pm 4\lambda_{ds} - 2\lambda_{SP}]$ |
| $\mathcal{C}_{S_I S_R Z'}$ | $\frac{2}{3} g_p (p_1 - p_2)^\mu$ |
| $\mathcal{C}_{S_{I(R)} S_{I(R)} Z' Z'}$ | $i16g_p^2$ |

TABLE I: Vertices related with $S_{I(R)}$ annihilation.

density and t3ps [54] to scan the parameter space. For simplicity, we assume $\lambda_s = 0$ since the self interaction part of dark matter makes no contribution to the relic density. Moreover, searches for the exotic Higgs at the LHC give upper limits of the mixing angle with $|\sin \theta| \leq 0.2 \sim 0.6$ depending on the heavy Higgs mass [55–57]. In addition, as we discussed above, M_{Z_p} and g_p are limited with current experiments. To sum up, there are 8 independent parameters in the model, and we take three Scenarios to estimate these parameters separately for simplicity. In *Scenario A*, we consider $(g - 2)_\mu$ anomaly as well as dark matter relic density constraint on the $M_{Z_p} - g_p$. In *Scenario B*, we discuss contribution of other parameters on the dark matter relic density. In *Scenario C*, we focus on the relic density constraint on the couplings λ_{Hs} , λ_{SP} and λ_{ds} .

Scenario A

In this part, we focus on $(g - 2)_\mu$ anomaly as well as dark matter relic density constraint on the $M_{Z_p} - g_p$, the inputs are set by Table II. According to Figure 6, we give the allowed region to satisfy relic density constraint (blue dots) and $(g - 2)_\mu$ anomaly (red region) with $M_{Z_p} \subseteq [0.01, 0.25]$ GeV and $g_p \subseteq [4 \times 10^{-4}, 0.002]$ where we have set $\sin \theta = 0.01$, $m_2 \subseteq [0.2, 2]$ TeV and $\lambda_{Hs, SP, ds} \subseteq [10^{-5}, 0.1]$. Since we have chosen m_2 and $v_b = M_{Z_p}/2g_p$ as inputs, these parameters should be limited by perturbative constraint as well as vacuum stability constraint, which means $v_b = M_{Z_p}/2g_p$ should not be too small. As we can see from Figure 6, most

| Parameter | value for inputs |
|----------------|-----------------------------|
| m_2 | [0.2, 2] TeV |
| $\sin \theta$ | 0.001 |
| λ_{Hs} | $[10^{-5}, 0.1]$ |
| λ_{SP} | $[10^{-5}, 0.1]$ |
| λ_{ds} | $[10^{-5}, 0.1]$ |
| M_{Z_p} | [0.01, 0.25] GeV |
| g_p | $[4 \times 10^{-4}, 0.002]$ |
| m_0 | [0, 60] GeV |

TABLE II: Values for the parameters as input to calculate dark matter relic density.

of the blue points fall in the lower-right region, and the upper-left region is excluded within the chosen parameter space.

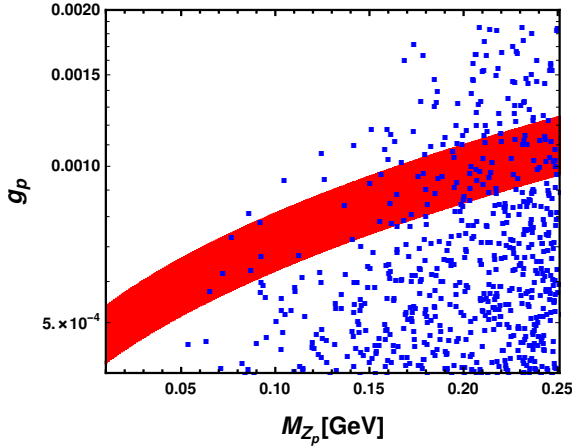


FIG. 6: Allowed $M_{Z_p} - g_p$ region to satisfy relic density constraint [blue dots] and $(g - 2)_\mu$ anomaly [red region] with $M_{Z_p} \subseteq [0.01, 0.25]$ GeV and $g_p \subseteq [4 \times 10^{-4}, 0.002]$ where we have set $\sin \theta = 0.01$, $m_2 \subseteq [0.2, 2]$ TeV and $\lambda_{Hs, SP, ds} \subseteq [10^{-5}, 0.1]$, $m_0 \subseteq [0, 60]$ GeV.

Scenario B

In this part, we discuss contribution of other parameters to the dark matter relic density. The results of relic density are shown in Figure 7, where curves with different color corresponding with one of the parameter varies. We set $0 \leq m_0 \leq 60$ GeV and benchmark value for the parameters are given in Table III. We fix $M_{Z_p} = 0.2$ GeV and $g_p = 0.001$ in Figure 7[first], while in Figure 7[second] we fix $M_{Z_p} = 0.1$ GeV and $g_p = 0.0007$.

According to Figure 7[first], the purple solid curve is the observed relic density at experiments. Curves corresponding to $m_2 = 600$ GeV and $\sin \theta = 0.03$ almost coincide with the benchmark curve, this is due to dark matter annihilation channels related with Higgs make little contribution to relic density in these cases.

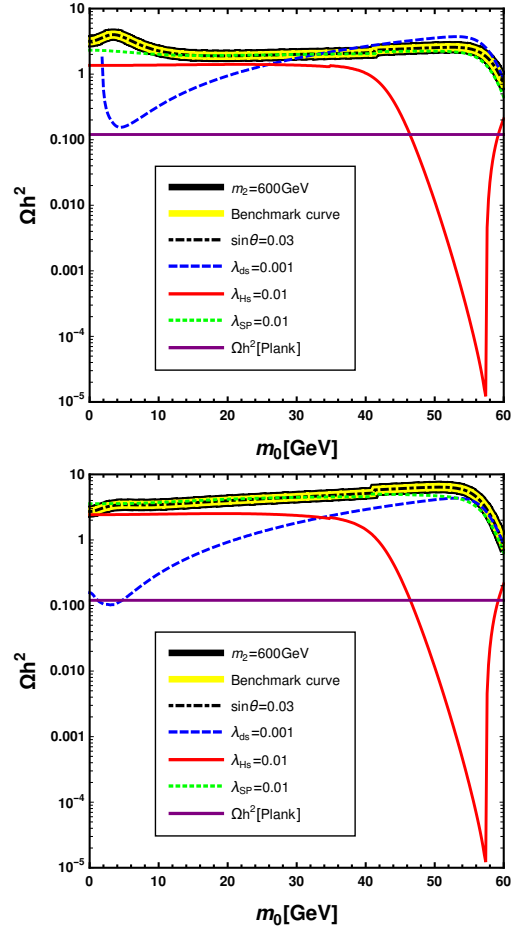


FIG. 7: The value of Relic density as function of m_0 . The purple solid curve is the observed relic density at experiment [50]. Curves with different color corresponding to different parameter varies when $M_{Z_p} = 0.2$ GeV, $g_p = 0.001$ [first figure] and $M_{Z_p} = 0.1$ GeV, $g_p = 0.0007$ [second figure].

| Parameter | benchmark value for inputs |
|----------------|----------------------------|
| m_2 | 300 GeV |
| $\sin \theta$ | 0.001 |
| λ_{Hs} | 1×10^{-4} |
| λ_{SP} | 1×10^{-4} |
| λ_{ds} | 1×10^{-4} |
| M_{Z_p} | 0.2 GeV |
| g_p | 0.001 |

TABLE III: Benchmark value for the parameters as input to calculate dark matter relic density.

Correspondingly, for the red line with $\lambda_{Hs} = 0.01$, we have a resonance region at about $2m_{DM} = m_1$, where the relic density drops sharply, and intersect with the relic density constraint curve. For $\lambda_{ds} = 0.001$, see the blue dashed curve, the dark matter mass can be negative when m_0 takes small value, so that the start point of the curve is not $m_0 = 0$. For Figure 7[second] with $M_{Z_p} = 0.1$ GeV and $g_p = 0.0007$, the curves are almost the same with those in Figure 7[first], and one of the typical difference is

that the blue dashed curve corresponding to $\lambda_{ds} = 0.001$ starts at $m_0 = 0$ and intersect with the relic density constraint curve. According to these figures, we can reduce the inputs to λ_{ds} , λ_{SP} , λ_{Hs} , m_0 , M_{Z_p} and g_p , since contribution of m_2 and $\sin \theta$ to relic density can be small.

Scenario C

| Parameter | value for inputs |
|----------------|-------------------|
| m_2 | 300 GeV |
| $\sin \theta$ | 0.001 |
| M_{Z_p} | 0.2 GeV |
| g_p | 0.001 |
| m_0 | [0, 60] GeV |
| λ_{Hs} | $[10^{-5}, 0.01]$ |
| λ_{SP} | $[10^{-5}, 0.01]$ |
| λ_{ds} | $[10^{-5}, 0.01]$ |

TABLE IV: values for the parameters as input to scan.

In this part, we scan the parameter space to study the relic density constraint on the couplings. For simplicity, we fix M_{Z_p} , g_p , $\sin \theta$, m_2 and focus on λ_{SP} , λ_{ds} as well as λ_{Hs} . We set these parameters as in Table IV. To avoid m_{DM} taking too large value, we have set the couplings $\lambda_{Hs, SP, ds}$ to be smaller than 0.01. The results are given in Figure 8. According to the first picture of Figure 8,

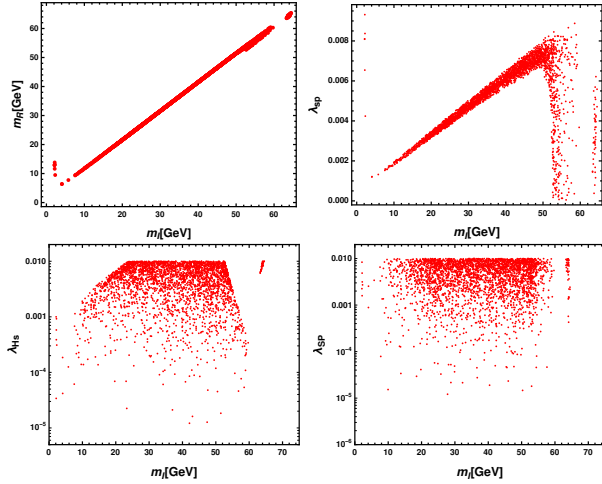


FIG. 8: Scatter points satisfying relic density constraint with the X-axis being S_I mass. Y-axis being S_R mass in the first figure. The scan results of $\lambda_{ds} - m_I$, $\lambda_{Hs} - m_I$ and $\lambda_{SP} - m_I$ are in the second, third and fourth figure respectively.

the possible dark matter S_I mass ranges from a few GeV to about $m_1/2$ as we discussed above, for m_I bigger than about 10 GeV, we have $m_R \approx m_I$ and $\Delta \approx 0$ which means co-annihilation process can be dominate in the evolution of relic density where both S_R and S_I play the role of dark matter. For S_I takes smaller value, Δ can

be much large and only S_I plays the role of dark matter, but such region is constrained stringently. In addition, we give the scan result of $\lambda_{ds} - m_I$, $\lambda_{Hs} - m_I$ and $\lambda_{SP} - m_I$ in the other figures in Figure 8 separately. As we can see from the second picture, the allowed value of λ_{ds} is constrained within a narrow region when m_I smaller than about 50 GeV, increasing with m_I increases, such result seemingly contraries to Eq.(9), where m_I decreases with λ_{ds} increase, this means λ_{Hs} and λ_{SP} play more important role determining dark matter mass under the relic density constraint. For $m_I > 50$ GeV, λ_{ds} can take value within the whole range of $[1 \times 10^{-5}, 0.0084]$. For λ_{Hs} and λ_{SP} in the last two picture, both can take value from 1×10^{-5} to 0.01, and a certain number of the points fall in the region $[0, 001, 0.01]$, with a few points obtained at low mass region.

C. Direct detection

Experiments related with dark matter direct detection such as CDMS II [58], XENON100 [59], XENON1T [60], LUX [61] have been searching for the signal of the interaction of DM with nucleon. In our model, quarks do not couple with Z' but only with two Higgs particles and these interactions can be concluded by the scattering of dark matter particle off a SM fermion f via the t-channel exchange of the two Higgs particles, which is similar with the two singlet scalar model [62, 63]. The effective lagrangian for dark matter-quark elastic scattering can be given by :

$$\mathcal{L}_{q,eff} = -\frac{m_q}{2v} \left(\frac{\mathcal{C}_{h_1 SS} \cos \theta}{m_1^2} + \frac{\mathcal{C}_{h_2 SS} \sin \theta}{m_2^2} \right) SS \bar{q} q, \quad (30)$$

and effective lagrangian related with S_I and S_R can be given by:

$$\mathcal{L}_{q,eff} = \sum_{S=S_R, S_I} -\frac{m_q}{2v} \left(\frac{\mathcal{C}_{h_1 SS} \cos \theta}{m_1^2} + \frac{\mathcal{C}_{h_2 SS} \sin \theta}{m_2^2} \right) SS \bar{q} q \quad (31)$$

Furthermore, the effective lagrangian related with DM-nucleon elastic scattering can be given by:

$$\mathcal{L}_{N,eff} = \sum_{S=S_R, S_I} \frac{m_N - \frac{7}{9}m_B}{v} \left(\frac{\mathcal{C}_{h_1 SS} \cos \theta}{m_1^2} + \frac{\mathcal{C}_{h_2 SS} \sin \theta}{m_2^2} \right) SS \bar{N} N \quad (32)$$

where m_N represents the nucleon mass and m_B represents the baryon mass in the chiral limit [37]. The total cross section for S-N elastic scattering can be given by:

$$\sigma_{SN \rightarrow SN} = \frac{m_N^4 f_N^2}{4\pi(m_N + m_{DM})^2} \times \left(\frac{\mathcal{C}_{h_1 SS} \cos \theta}{m_1^2} + \frac{\mathcal{C}_{h_2 SS} \sin \theta}{m_2^2} \right)^2, \quad (33)$$

where f_N is the Higgs-nucleon Formfactor with $f_N = 0.308(18)$ according to the phenomenological and lattice-QCD calculations [64] and m_{DM} corresponds to both m_I and m_R .

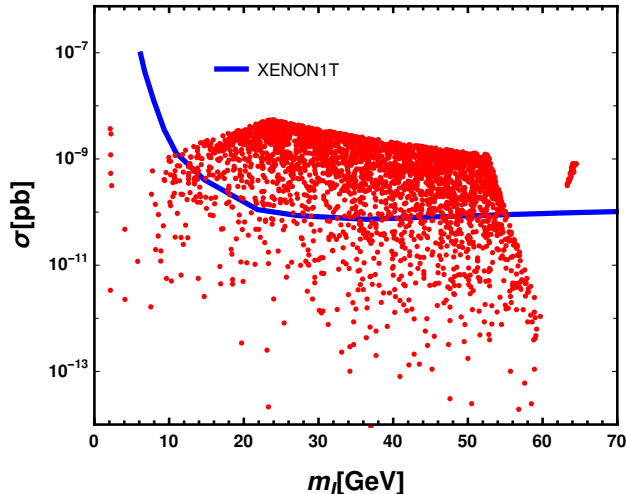


FIG. 9: Spin independent cross section as a function of m_I , the red points represent result of the chosen parameter space satisfying relic density constraint, the blue dashed curve represents result of XENON1T [60].

We consider the direct detection constraint on the chosen parameter space of the model and the result is given in Figure 9, where the plot is drawn as a function of m_I . The blue dashed curve in Figure 9 represents result of XENON1T [60] and the red points represent result of the chosen parameter space satisfying relic density constraint. According to Figure 9, although a certain number of the red points fall above the region of direct detection constraint, which means these points are excluded by direct detection constraint. There remain points that mass ranging from a few GeV to about 60 GeV to both satisfy relic density constraint as well as direct detection constraint. In other word, while direct detection can give stringent limit on the parameter space, dark matter mass can be from a few GeV to about 60 GeV within a viable parameter space satisfying relic density constraint in the model.

V. SUMMARY

SM has achieved great success for its high accuracy to describe electroweak and strong interaction. However, there remains problems such as neutrino mass and

dark matter that SM can not explain. In addition, recent results about muon anomalous magnetic moment $(g-2)_\mu$ brings new challenges to the SM. The 4.2σ discrepancy between experiment and SM prediction seems to indicate new physics behind $(g-2)_\mu$ anomaly and gives possible hints to the Beyond SM physics. Among these models, a gauged $U(1)_{L_\mu-L_\tau}$ model stands out for its simplicity since the gauge anomaly cancellation can be accomplished without introducing extra fermions. Related discussion about such model and experiment constrain the new gauge boson Z' mass at MeV scale, which also satisfying the $(g-2)_\mu$ constraint. In addition, one can also introduce new particles to the $L_\mu-L_\tau$ model so that dark matter problem as well as neutrino mass problem can both be explained.

In this article, we consider a scalar dark matter model within the frame of a gauged $L_\mu-L_\tau$ model. We introduce a new gauge boson Z' as well as two scalar fields S and Φ to the SM. The lighter component of S can play the role of dark matter which is stabilized by the residual Z_2 symmetry after spontaneously symmetry breaking. In this work, we focus on dark matter and $(g-2)_\mu$ anomaly and ignore the neutrino mass problem. In the case of $m_I < m_1/2$, $m_R < m_1/2$ and $M_{Z_p} < m_1/2$, we have new Higgs invisible channels which should be limited by current experiment result at LHC. A viable parameter space is considered to discuss the possibility of light dark matter as well as co-annihilation case. We consider relic density constraint and find in the case of m_I taking a few GeV, we can have the imaginary part S_I of S as light dark matter with m_R much larger than m_I , but the allowed parameter space is constrained stringently. However, with m_I increasing, the allowed value for m_I and m_R is approximately equal so that we have $\Delta \approx 0$, and we come to so-called co-annihilation process, where both S_R and S_I play the role of dark matter. At low mass region, relic density constraint limits λ_{ds} stringently, which plays a significant role determining m_I and m_R . In addition, direct detection has also been taken into consideration to constrain the chosen parameter space, and the spin-independent dark matter nucleon elastic scattering cross section can give stringent constraint the viable parameter space. As we discussed above, we have shown this model can explain dark matter and $(g-2)_\mu$ anomaly at the same time in certain parameter space.

Acknowledgments

Hao Sun is supported by the National Natural Science Foundation of China (Grant No.12075043).

-
- [1] B. Abi et al. (Muon $g-2$), Phys. Rev. Lett. **126**, 141801 (2021), 2104.03281.
 - [2] T. Albahri et al. (Muon $g-2$), Phys. Rev. A **103**, 042208

- (2021), 2104.03201.
- [3] T. Albahri et al. (Muon $g-2$), Phys. Rev. D **103**, 072002 (2021), 2104.03247.

- [4] J. Kawamura, S. Okawa, and Y. Omura, JHEP **08**, 042 (2020), 2002.12534.
- [5] P. Athron, C. Balázs, D. H. Jacob, W. Kotlarski, D. Stöckinger, and H. Stöckinger-Kim (2021), 2104.03691.
- [6] E. A. Baltz and P. Gondolo, Phys. Rev. Lett. **86**, 5004 (2001), hep-ph/0102147.
- [7] L. L. Everett, G. L. Kane, S. Rigolin, and L.-T. Wang, Phys. Rev. Lett. **86**, 3484 (2001), hep-ph/0102145.
- [8] D. Choudhury, B. Mukhopadhyaya, and S. Rakshit, Phys. Lett. B **507**, 219 (2001), hep-ph/0102199.
- [9] K.-m. Cheung, Phys. Rev. D **64**, 033001 (2001), hep-ph/0102238.
- [10] X. Calmet and A. Neronov, Phys. Rev. D **65**, 067702 (2002), hep-ph/0104278.
- [11] Z.-H. Xiong and J. M. Yang, Phys. Lett. B **508**, 295 (2001), hep-ph/0102259.
- [12] P. Cox, C. Han, and T. T. Yanagida (2021), 2104.03290.
- [13] N. Chakrabarty, C.-W. Chiang, T. Ohata, and K. Tsumura, JHEP **12**, 104 (2018), 1807.08167.
- [14] N. Chakrabarty (2020), 2010.05215.
- [15] R. Foot, X. G. He, H. Lew, and R. R. Volkas, Phys. Rev. D **50**, 4571 (1994), hep-ph/9401250.
- [16] W. Altmannshofer, C.-Y. Chen, P. S. Bhupal Dev, and A. Soni, Phys. Lett. B **762**, 389 (2016), 1607.06832.
- [17] P. Foldenauer and J. Jaeckel, JHEP **05**, 010 (2017), 1612.07789.
- [18] S. Baek, N. G. Deshpande, X. G. He, and P. Ko, Phys. Rev. D **64**, 055006 (2001), hep-ph/0104141.
- [19] X. G. He, G. C. Joshi, H. Lew, and R. R. Volkas, Phys. Rev. D **43**, 22 (1991).
- [20] X.-G. He, G. C. Joshi, H. Lew, and R. R. Volkas, Phys. Rev. D **44**, 2118 (1991).
- [21] G. Bélanger, C. Delaunay, and S. Westhoff, Phys. Rev. D **92**, 055021 (2015), 1507.06660.
- [22] J. Heeck and W. Rodejohann, Phys. Rev. D **84**, 075007 (2011), 1107.5238.
- [23] J. P. Lees et al. (BaBar), Phys. Rev. D **94**, 011102 (2016), 1606.03501.
- [24] S. R. Mishra et al. (CCFR), Phys. Rev. Lett. **66**, 3117 (1991).
- [25] Y. Kaneta and T. Shimomura, PTEP **2017**, 053B04 (2017), 1701.00156.
- [26] E. J. Chun, A. Das, J. Kim, and J. Kim, JHEP **02**, 093 (2019), [Erratum: JHEP 07, 024 (2019)], 1811.04320.
- [27] E. Komatsu et al. (WMAP), Astrophys. J. Suppl. **192**, 18 (2011), 1001.4538.
- [28] H.-Y. Chiu, Phys. Rev. Lett. **17**, 712 (1966).
- [29] L. J. Hall, K. Jedamzik, J. March-Russell, and S. M. West, JHEP **03**, 080 (2010), 0911.1120.
- [30] G. Bélanger, K. Kannike, A. Pukhov, and M. Raidal, JCAP **06**, 021 (2014), 1403.4960.
- [31] M. J. Baker et al., JHEP **12**, 120 (2015), 1510.03434.
- [32] P. Foldenauer, Phys. Rev. D **99**, 035007 (2019), 1808.03647.
- [33] W. Altmannshofer, S. Gori, S. Profumo, and F. S. Queiroz, JHEP **12**, 106 (2016), 1609.04026.
- [34] A. Biswas, S. Choubey, and S. Khan, JHEP **02**, 123 (2017), 1612.03067.
- [35] P. Das, M. K. Das, and N. Khan (2021), 2104.03271.
- [36] K. Cheung, Y.-L. S. Tsai, P.-Y. Tseng, T.-C. Yuan, and A. Zee, Nucl. Phys. B Proc. Suppl. **246-247**, 116 (2014).
- [37] X.-G. He, T. Li, X.-Q. Li, J. Tandean, and H.-C. Tsai, Phys. Rev. D **79**, 023521 (2009), 0811.0658.
- [38] C.-W. Chiang, T. Nomura, and J. Tandean, Phys. Rev. D **87**, 073004 (2013), 1205.6416.
- [39] Y. Farzan and A. R. Akbarieh, JCAP **10**, 026 (2012), 1207.4272.
- [40] Y. Farzan and A. R. Akbarieh, JCAP **11**, 015 (2014), 1408.2950.
- [41] A. Biswas, S. Choubey, and S. Khan, JHEP **09**, 147 (2016), 1608.04194.
- [42] N. Chakrabarty, D. K. Ghosh, B. Mukhopadhyaya, and I. Saha, Phys. Rev. D **92**, 015002 (2015), 1501.03700.
- [43] K. Kannike, Eur. Phys. J. C **76**, 324 (2016), [Erratum: Eur.Phys.J.C 78, 355 (2018)], 1603.02680.
- [44] A. Biswas, S. Choubey, and S. Khan, JHEP **08**, 114 (2016), 1604.06566.
- [45] M. Agostini et al. (Borexino), Phys. Rev. D **100**, 082004 (2019), 1707.09279.
- [46] M. Abdullah, J. B. Dent, B. Dutta, G. L. Kane, S. Liao, and L. E. Strigari, Phys. Rev. D **98**, 015005 (2018), 1803.01224.
- [47] W. Altmannshofer, S. Gori, M. Pospelov, and I. Yavin, Phys. Rev. Lett. **113**, 091801 (2014), 1406.2332.
- [48] M. Tanabashi et al. (Particle Data Group), Phys. Rev. D **98**, 030001 (2018).
- [49] E. W. Kolb and M. S. Turner, Nature **294**, 521 (1981).
- [50] N. Aghanim et al. (Planck), Astron. Astrophys. **641**, A6 (2020), 1807.06209.
- [51] K. Griest and D. Seckel, Phys. Rev. D **43**, 3191 (1991).
- [52] A. Alloul, N. D. Christensen, C. Degrande, C. Duhr, and B. Fuks, Comput. Phys. Commun. **185**, 2250 (2014), 1310.1921.
- [53] G. Bélanger, F. Boudjema, A. Goudelis, A. Pukhov, and B. Zaldivar, Comput. Phys. Commun. **231**, 173 (2018), 1801.03509.
- [54] V. Maurer, Comput. Phys. Commun. **198**, 195 (2016), 1503.01073.
- [55] E. Accomando, C. Coriano, L. Delle Rose, J. Fiaschi, C. Marzo, and S. Moretti, JHEP **07**, 086 (2016), 1605.02910.
- [56] T. Robens and T. Stefaniak, Eur. Phys. J. C **75**, 104 (2015), 1501.02234.
- [57] D. López-Val and T. Robens, Phys. Rev. D **90**, 114018 (2014), 1406.1043.
- [58] Z. Ahmed et al. (CDMS-II), Science **327**, 1619 (2010), 0912.3592.
- [59] E. Aprile et al. (XENON), Phys. Rev. Lett. **119**, 181301 (2017), 1705.06655.
- [60] E. Aprile et al. (XENON), JCAP **04**, 027 (2016), 1512.07501.
- [61] D. Akerib et al. (LUX), Phys. Rev. Lett. **112**, 091303 (2014), 1310.8214.
- [62] A. Abada, D. Ghaffor, and S. Nasri, Phys. Rev. D **83**, 095021 (2011), 1101.0365.
- [63] T. Basak, B. Coleppa, and K. Loho (2021), 2105.09044.
- [64] M. Hoferichter, P. Klos, J. Menéndez, and A. Schwenk, Phys. Rev. Lett. **119**, 181803 (2017), 1708.02245.